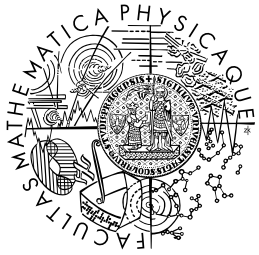

FACULTY
OF MATHEMATICS
AND PHYSICS
Charles University

BACHELOR THESIS

Andrej Farkaš

Investigation of electrical conductivity of thin films under influence of mechanical strain

Katedra chemické fyziky a optiky

Supervisor of the bachelor thesis:	prof. RNDr. Petr Němec, Ph.D.
Consultant of the bachelor thesis:	Mgr. Kamil Olejník, Ph.D.
Study programme:	Physics
Study branch:	General physics

Prague 2019

I declare that I carried out this bachelor thesis independently, and only with the cited sources, literature and other professional sources.

I understand that my work relates to the rights and obligations under the Act No. 121/2000 Sb., the Copyright Act, as amended, in particular the fact that the Charles University has the right to conclude a license agreement on the use of this work as a school work pursuant to Section 60 subsection 1 of the Copyright Act.

In ..... date ..... signature of the author

I would like to thank prof. RNDr. Petr Němec, Ph.D. for supervising my work and giving helpful suggestions concerning my thesis. Another irreplaceable scientist who guided me along the course of this work is Mgr. Kamil Olejník, Ph.D. and I would like to thank him for his assistance. My gratitude also goes to Ing. Vít Novák, CSc. for supplying the substrates for my samples. Lastly I would like to thank to all employees of Institute of Physics CAS at Cukrovarnická street for their patience and helpful nature.

Title: Investigation of electrical conductivity of thin films under influence of mechanical strain

Author: Andrej Farkaš

Katedra: Katedra chemické fyziky a optiky

Supervisor: prof. RNDr. Petr Němec, Ph.D., Katedra chemické fyziky a optiky

Abstract: Magnetization of atiferromagnetic devices can be manipulated electrically or mechanically. In order to do mechanical manipulation specialized device was constructed and tested with cross structure on three different thin metal layers comparable to antiferromagnetic devices on top of the most common substrates GaAs and GaP. Results of said testing proved machine is usable for intended purpose, with few tweaks.

Keywords: Conductivity Strain Bending Mechanical design Spintronics Lithography

Contents

Introduction

Main goal of this work is to create and test a simple-to-use device capable of inducing strain in thin layers deposited on different substrates.

The tool is intended for testing spintronic microstructures (devices). The design is developed for automated operation (programmable application of strain while varying other testing parameters) and simple sample replacement allowing tests of numerous devices.

This thesis is divided into six chapters. First chapter describes strain induced changes in resistance and our motivation to use this machine on antiferromagnetic devices with strain assisted operation. Machine designed for this purpose with all of its parts and programming is described in the second chapter. Third chapter deals with computer simulations of bending effects created by our machine and it is intertwined with the design part mentioned in chapter two. In the chapter number 4 we focus on sample creation with all of the steps including substrate preparation, lithography and metal deposition. The fifth chapter is dedicated to measurement and its results and processing. And finally the last, sixth, chapter is giving future suggestions for improvement and tries to resolve encountered issues.

1. Electrical measurements of thin layers with applied strain

1.1 Strain induced changes in resistivity of metals

This phenomenon is well known and it is already employed in many devices around us. It uses a simple principle. Where resistance R of a metal wire is determined by electric resistivity ρ, length l and wire's cross-section A.

$$R = \rho \frac{l}{A} \tag{1.1}$$

Simple device using strain as a factor in changing the resistance of a wire was reported by Lord Kelvin in 1856 as he saw increase in wire's resistance with increasing strain and decrease of resistance with decreasing strain.

Change in resistance is combination of changes in length, cross-section area and resistivity [1].

$$dR = \frac{\rho}{A} dl - \frac{\rho l}{A^2} dA + \frac{l}{A} d\rho \tag{1.2}$$

$$\frac{dR}{R} = \frac{dl}{l} - \frac{dA}{A} + \frac{d\rho}{\rho} \tag{1.3}$$

If we try to break apart every effect contributing to change in resistance of a wire with strain we will see three effects. Strain can be represented in 1D as relative change in length [2].

$$\varepsilon_l = \frac{dl}{l} \tag{1.4}$$

However, change in length is not the only effect. We need to look at the change of cross-section of a wire. If we think of cylindrical wire with radius r, cross-section will also change due to Poisson's ratio. We can determine radial strain as:

$$\varepsilon_r = \frac{dr}{r} = -\nu \varepsilon_l = -\nu \frac{dl}{l} \tag{1.5}$$

Then the change rate of a wire's cross-section is determined as (approximation works only for small strains):

$$\frac{dA}{A} = (1 + \varepsilon_r)^2 - 1 = 2\varepsilon_r + \varepsilon_r^2 \approx 2\varepsilon_r = -2\nu \frac{dl}{l} \tag{1.6}$$

Combining all of the above equations we can write resistance change rate as:

$$\frac{dR}{R} = \frac{dl}{l} - \frac{dA}{A} + \frac{d\rho}{\rho} = (1 + 2\nu)\frac{dl}{l} + \frac{d\rho}{\rho} = (1 + 2\nu)\varepsilon_l + \frac{d\rho}{\rho} \tag{1.7}$$

Now we can calculate sensitivity S or sometimes called Gauge factor GF for a given material following this equation:

$$S = \frac{dR/R}{\varepsilon_l} = 1 + 2\nu + \frac{d\rho/\rho}{\varepsilon_l} \tag{1.8}$$

This sensitivity can be now used to represent relative change in resistance as:

$$\frac{dR}{R} = S\varepsilon \tag{1.9}$$

One of our goal is to evaluate sensitivity for thin layers of few different metals. Because from theory we know, that the relative change in resistance is linearly dependent on strain and from simulations we know that strain in x axis is dominant in the center area of a sample, we can evaluate response of our machine. Because any flexing in the machine will present itself in change of linearity of the strain/resistance curve. For that we want to use materials with known sensitivity. This sensitivity can be found in Table 1.1 . We will be using pure Nickel and Nichrome as our baseline materials.

Table 1.1: Sensitivity S or Gauge factor GF of different materials

Material	Sensitivity S (GF)
Platinum (Pt 100%)	6,1
Nickel (Ni 100%)	-12,1
Nichrome V (Ni 80%, Cr 20%)	2,1
Constantan (Ni 45%, Cu 55%)	up to 200
Silicon	up to 200

1.1.1 Practical application - Strain gauge

In real-world applications we can encounter using this phenomenon in so called strain gauges. In order to maximize the relative resistance change they use special pattern to prolong used wire in order accumulate length change, help dissipate any heat created by stretching and to determine sensitivity of a strain gauge - uni-axial, bi-axial or multi-axial. Material used in strain gauges is typically Constantan, which resistance, sensitivity and thermal dependency are a good compromise. Examples of few types of strain gauges can be found on Fig. 1.1.

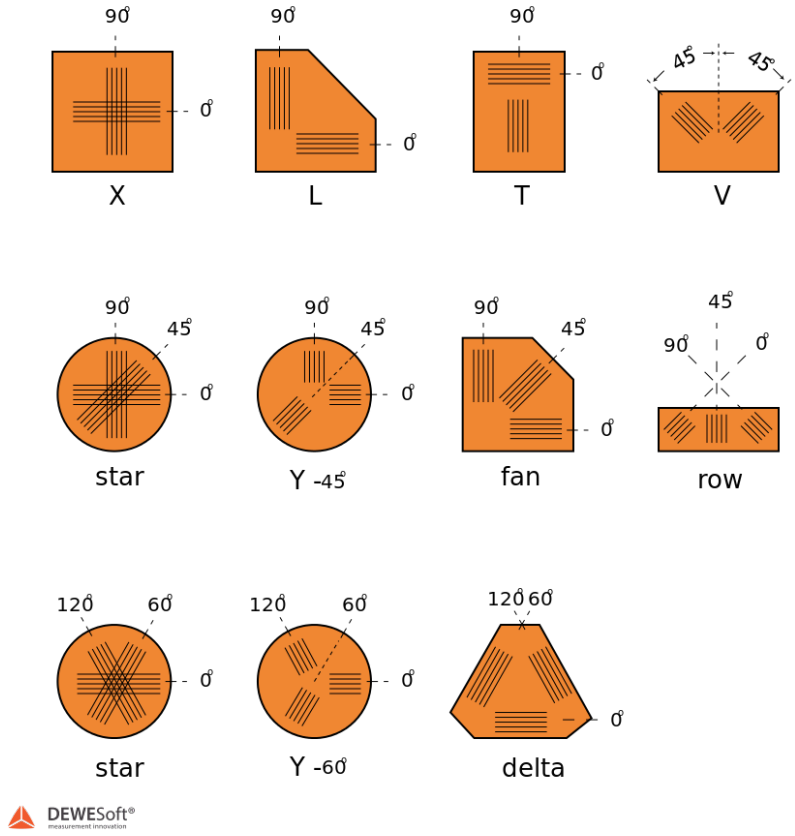

Figure 1.1: Different commercial types and patterns of strain gauges.

1.2 Four point and Van der Pauw method of measuring resistance

Usually the most common method of measuring resistance is two point method. This method utilizes simple multimeter function or if we break down that function it uses voltage source and ammeter and from that resistance is calculated via Ohm's law [3].

In order to avoid several obvious problems like contact resistance, wire resistance and geometry, four point method was developed. It utilizes measurement of potential difference between two points, while defined electrical current flows through the active region by its separate contacts. Four point method is illustrated on Fig. 1.2. Important characteristic of four point method is that we can calculate resistance of the sample without knowing resistance of wires and contacts. Because negligible current flows through the voltmeter, (it has at least 10^5 magnitude higher impedance than sample) and wires connected to a current source are in series with the sample, so the current through the whole loop is the same [3].

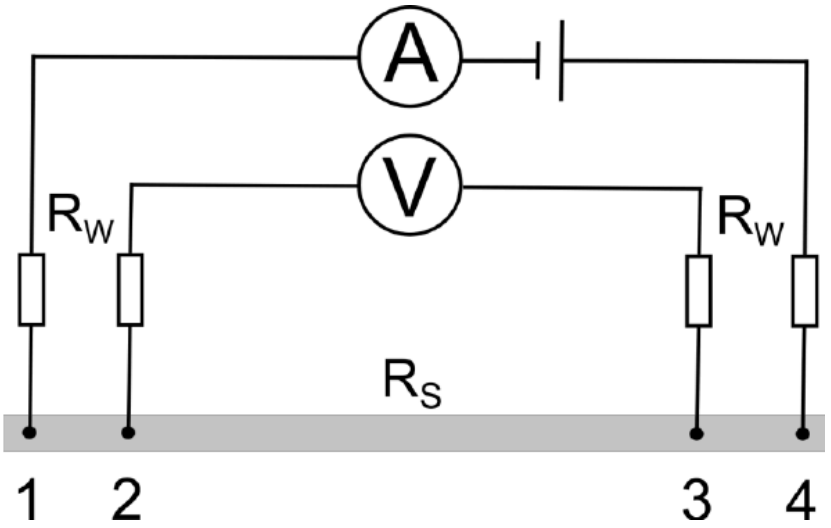

Figure 1.2: Schematic of four point measurement technique.

The four-point resistance measurement method commonly used to measure resistance assumes that the material sample has rectangular thin film geometry. If we want to measure samples of arbitrary shape, with no need to measure physical dimensions of said shape we have to use more general four-point resistivity measurement method called vad der Pauw method [3].

Four conditions have to be met before using van der Pauw method :

1. The sample must have flat shape of uniform thickness.
2. The sample must be free from any isolated holes.
3. The sample must be homogeneous and isotropic.
4. All four contacts must be located at the edges of the sample.

Simple example of utilized geometry and our application of van der Pauw method is on Fig. 1.3. Figure represents directions of current and readout voltage along the strain applied to the sample. Then we calculate resistance as:

$$R = \frac{V_{CD}}{I} \tag{1.10}$$

In order to get sheet resistance we need to multiply calculated resistance R by quotient:

$$R_s = \frac{\pi R}{ln2} \tag{1.11}$$

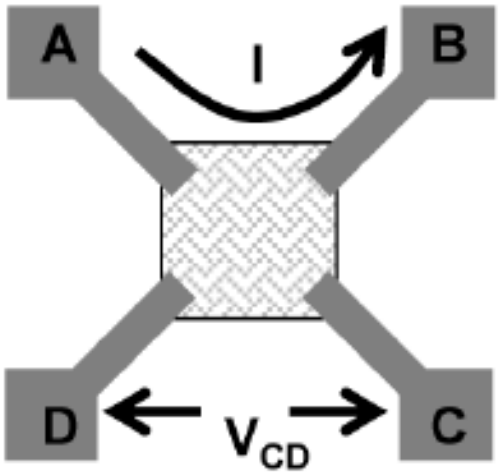

Figure 1.3: Schematic of utilized van der Pauw method along strain in horizontal direction.

1.3 Measurement geometry

The van der Pauw method described in previous section will be used in our setup. The sample geometry is shown in Fig. 1.4. The central cross is the active (van der Pauw) region of the sample, red circles indicate positions of contact needles.

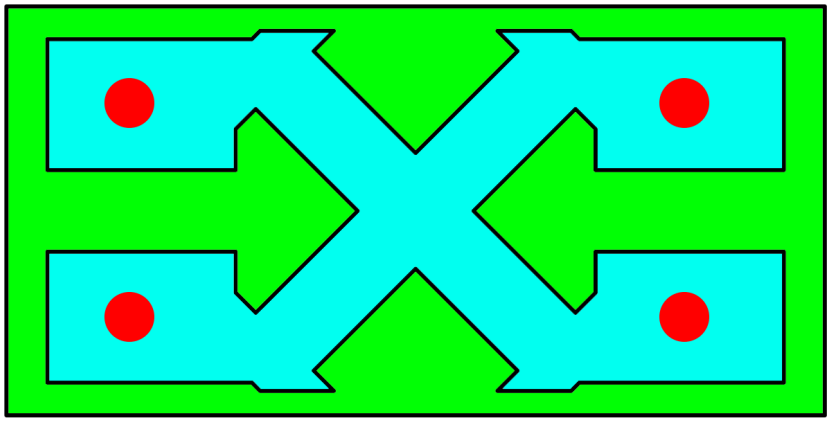

Figure 1.4: Top view of sample geometry. On top of substrate (Green) is thin layer (Cyan) with active region in central cross with contact needles (Red) on the sides.

The sample is strained by substrate bending in the geometry indicated in the side view of the sample shown in Fig. 1.5. The conductive layer is in the bottom side of the substrate, red needles are the four contact needles and black arrow indicate the applied force.

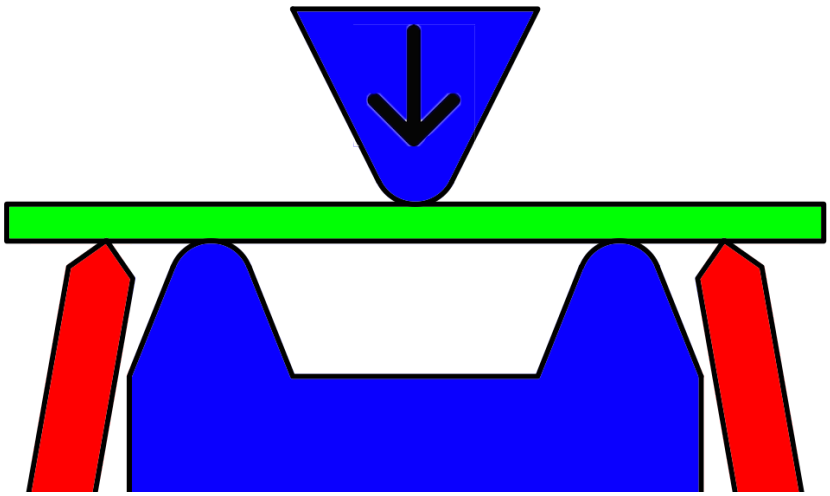

Figure 1.5: Side view of geometry used in our design. Sample (Green) is bent by metal parts (Blue) with force applied along the arrow. Spring loaded contacts (Red) are on the side of the sample.

1.4 Application in antiferromagnetic spintronics

Antiferromagnets are materials with alternating magnetic moment's directions. This results in their zero net magnetization. This creates few cornerstone advantages to antiferromagnets. Any information stored in spintronic devices is immune to electric charge perturbations compared to traditional charge based devices. And using antiferromagnets protects information even from magnetic field perturbations compared to spintronic devices on ferromagnets. Moreover, antiferromagnetic devices promises higher speed compared to traditional ferromagnetic devices. But they have key disadvantage - antiferromagnets are hard to control by an external magnetic field, therefore manipulation of moments (writing information) is more difficult.

Recently, this issue was resolved by discovery of current induced staggerd spin orbit fields capable of manipulation of antiferromagnetic moments allowing for construction of antiferromagnetic memory device and opening new subfield of antiferromagnetic spintronics [4],[5].

One of few other possible tools to manipulate (or assist manipulation of) magnetization antiferromagnetis is strain by utilizing the effect of magnetostriction. These future experiments are the motivation for construction of the strain inducing tool presented and tested in this work.

2. Creation of automated experimental setup

This chapter will deal with the motivation, technical details and process of construction of our automated experimental setup. Our goals were simple:

1. Construct a machine that can induce mechanical strain in samples.
2. Design it with ease of operation - contacting without glue or soldering, automated operation.
3. Create samples with possibility of creating different microdevices in the strained area.
4. Do so without being too complex or expensive.

Therefore we used commercially available parts and 3D printing. We also chose to use standard substrates like GaP and GaAs with dimensions 10x5mm allowing us to create microdevices in their centre. We knew we would need at least 4 contact points (Van der Pauw measurement).

2.1 Mechanical construction of the experimental setup

Firstly we tried to bend few samples using simple 3D printed forms squeezed together by screwing a bolt. This proved that bending samples of material currently being tested in our research group - CuMnAs can induce noticeable change of conductivity.

In order to improve reproducibility of strain induced in sample we chose to use mechanical linear actuator. We have been thinking about the idea of using piezoelectric actuators, which are more precise and do not posses any dead movement, compared to any mechanical machine. But they are limited in their range of movement and as simulations showed it would not have been sufficient.

To be able to calculate strain induced in thin layer on substrate with known thickness we need to be able to measure exact pushing movement of our machine. In order to do that we decided to use trapezoidal screws with 1mm pitch, which are known for their little dead movement and stepper motor with very fine steps of only 0,9°[6]. This means that theoretically we should be able to achieve smallest movement of 2,5 μm. But that is a theory, due to mechanical tolerances we cannot simply declare our positioning accuracy as that number. With some advanced software and hardware trickery, we are able to divide one full motor step into up to 256 microsteps [7] which can give us some more precision, but in practice 2,5 μm should be sufficient for our measurement.

For our bending surface we chose to use square 5x5 mm, which is determined by width of our samples and spacing of the edges, which is 5 mm. Due to manufacturing abilities of used CNC router in company Vakuum Praha, we rounded the edge with radius 0,5 mm. Manufacturing abilities are not the only reason

behind this decision. As our simulations have proven, rounded edge has the ability to better distribute contact stress in our sample, therefore we will avoid premature breaking of the samples. In our next iteration we want to apply long lasting non-conductive surface of SiO_2. In order to be able to do so, we cannot use sharp edge, but rounded one. Last big problem with sharp edges is the fact, that we want to bend samples and not to cut them. If the edges were too sharp they will act as a point of the highest pressure which will result in breaking of sample prematurely. In this first iteration of our machine we used simple spray on non-conductive coating to treat our edges.

Need of having sample supporting structures non-conductive have risen from decision of moving contacts outside of straining area. This decision was made upon preliminary testing which showed that bonding as well as soldering of our contacts is making substrates more fragile. We chose to use so called pogo pins or testing probes which are spring loaded contacts. Moving them outside of straining area helps to prolong durability of our substrates to achieve highest possible strain before breaking.

Whole design was based on simple linear motion stage. We chose design with two guiding rails and one driving shaft connected to a stepper motor via coupling. This linear motion is smooth thanks to usage of linear ball bearings. Possible range of travel is 18 mm, which is more than adequate for easy sample installation.

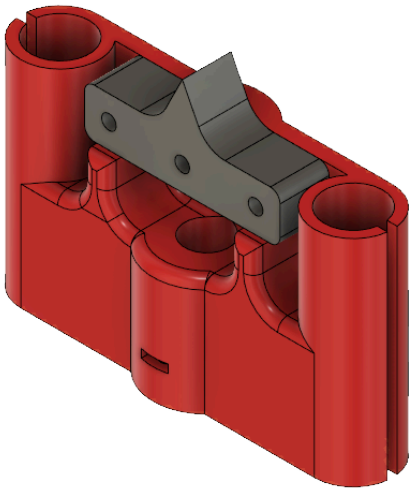

Figure 2.1: Design of moving stage with plastic (red) and stainless steel (grey) parts

Almost all parts were printed on a 3D FDM printer, namely Prusa i3 Mk2s,

with 0,15mm layer height using Prusament PLA, which is suitable plastic for this application due to its higher tensile modulus compared to other common 3D printing materials like PETG. [8]

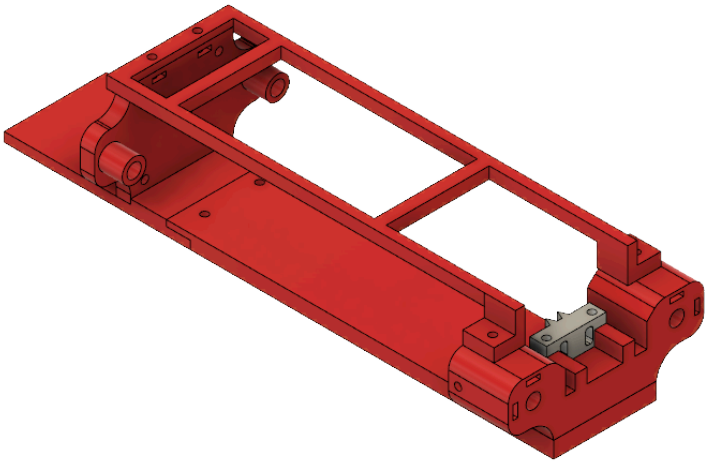

Figure 2.2: Design of stationary stage with plastic (red) and stainless steel (grey) parts

2.2 Microscope analysis of contact surfaces

After receiving final contact parts made by Vakuum Praha we decided to evaluate their roughness in electron microscope. In the electron microscope we were pleased with their surface. With only few defects around 30 μm in size maximum. As we can see on the Fig. 2.3 and 2.4 rounded edge has a decent quality with most of the marks parallel to the direction of the edge, which does not constitute a potential breakage point. Then we compared pictures of the same edges with optical microscope using magnification 10x. When comparing Fig. 2.5 to Fig. 2.3 and 2.4 we can see more defects and imperfections made by CNC router. It is interesting, that looking through electron microscope they are not that visible as in optical microscope.

Lastly we looked at the sharp edged parts inside electron as well as optical microscope. We can see on Fig. 2.6 that width of the edge is just 52 μm with only few defects. We can also see parallel lines present, which proves that both parts were made on the same machine leaving same marks. Comparing Fig. 2.6 and 2.7 we can see said marks on the sharp edge.

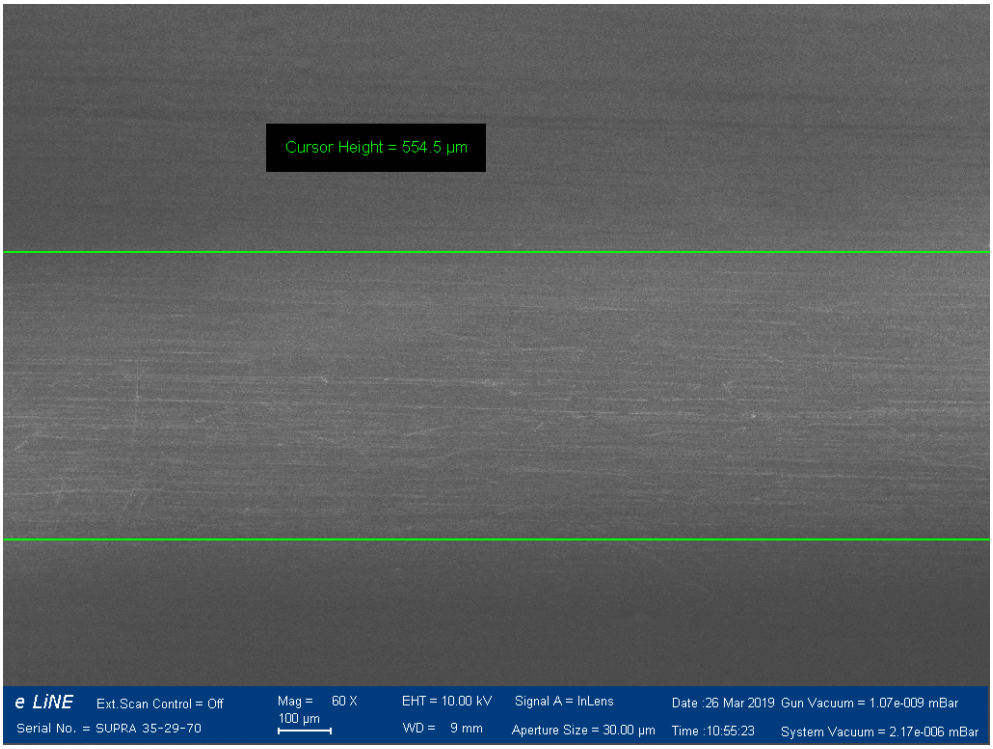

Figure 2.3: Electron microscope image of rounded contact surface. We can see mostly smooth surface with only parallel lines with the edge.

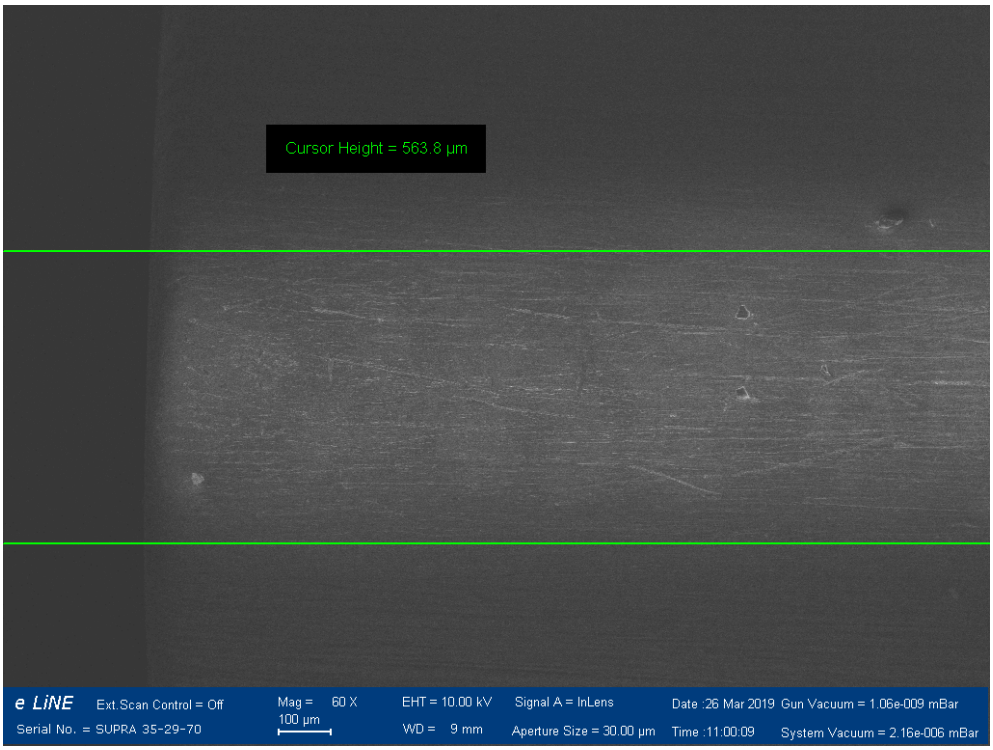

Figure 2.4: Electron microscope image of rounded contact surface. We can see the end of the surface and also few defects.

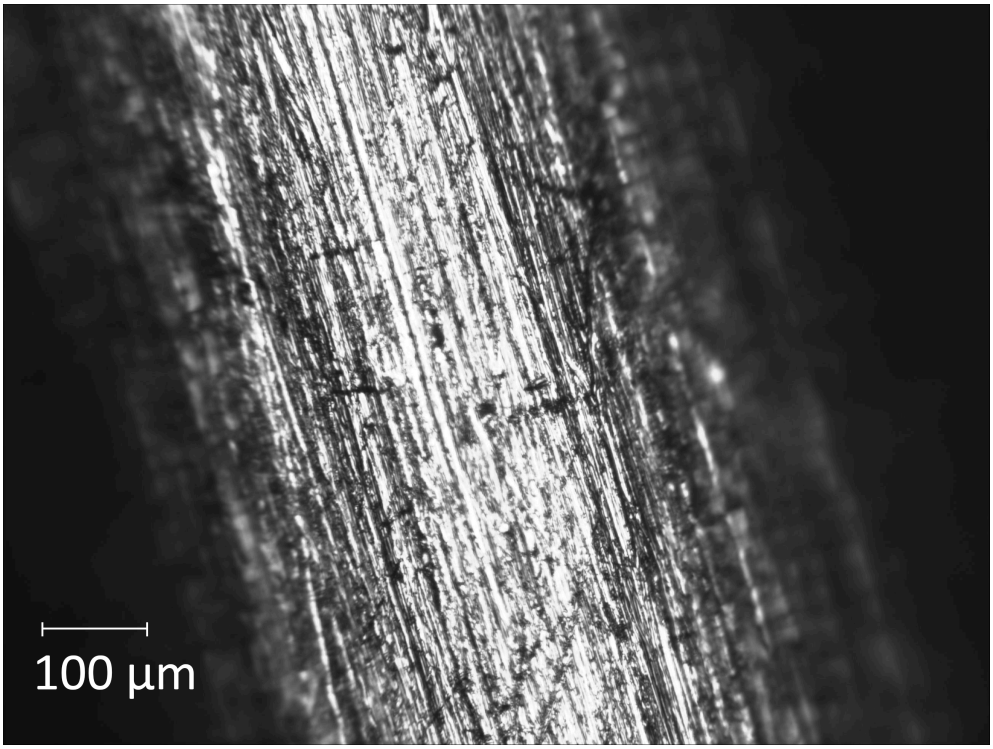

Figure 2.5: Optical microscope image of rounded contact surface with 10x magnification. We can see more small defects on the surface.

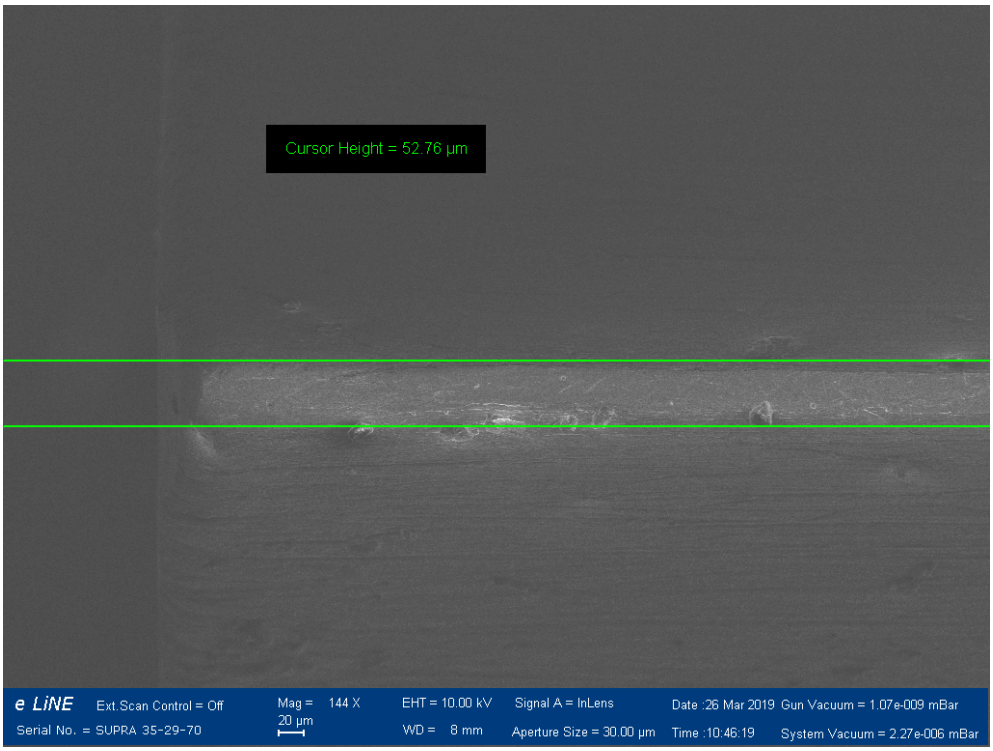

Figure 2.6: Electron microscope image of sharp contact surface.

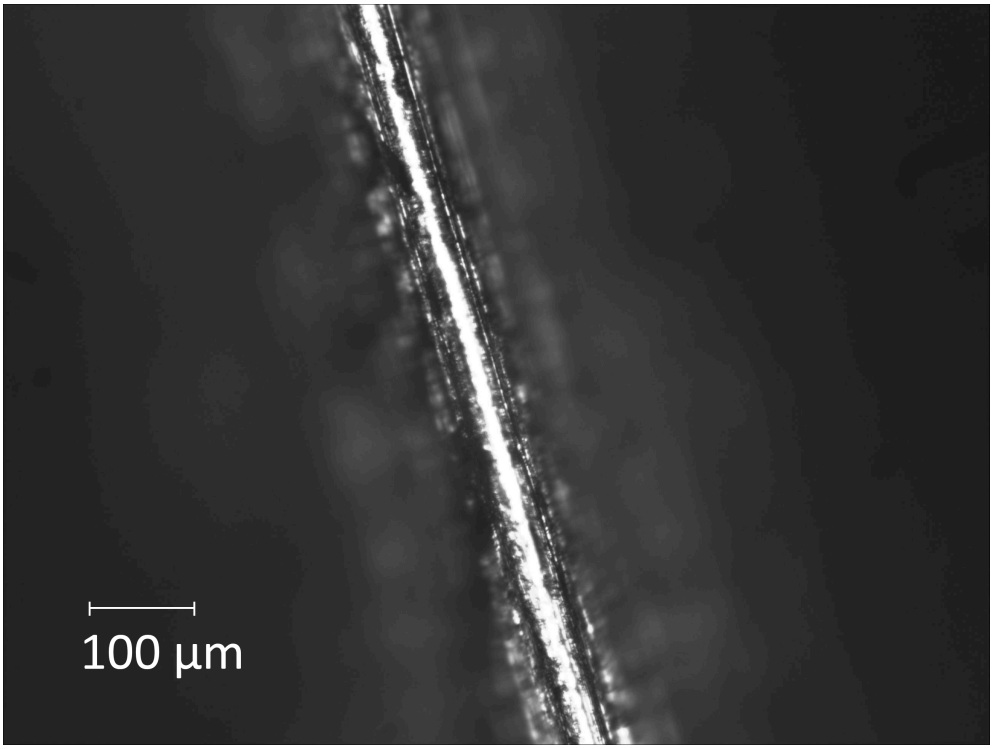

Figure 2.7: Optical microscope image of sharp edge using 10x magnification.

2.3 Programming and function overview of our machine

Our goals were quite achievable in theory, but as it was proven, not every manufacturer states realistic capabilities of their products in its datasheets.

First of all we needed to establish link between arduino micro-controller and stepper motor driver. We chose to use Arduino Uno and Trinamic TMC 2130 stepper motor driver as our devices. We chose this combination because of load sensing capability incorporated into TMC 2130 driver. During standard use of such stepper motor drivers micro-controller is not provided with any feedback from the driver. It supplies only STEP signal, which is a signal comprised of microsecond square wave pulses. Every pulse means rotation of one step or microstep, if microstepping is used. Another signal is just high or low logical level providing signal about rotation direction. We wanted a feedback system from our driver to the micro-controller. Therefore we chose to use more advanced driver which incorporates serial data communication. With that we can access registers on board the TMC 2130 chip [7]. In these registers we can monitor the driver's failures - overheating, over-current, reverse polarity etc. as well as driver's status - motor load, stall detection, missed steps. In order to create reliable measurement we need to be able to detect at least missed steps.

We wanted to use also advanced measurement provided by the stepper motor driver - motor load measurement. This should be able to allow us to create auto-homing function. This function would move down slowly towards the sample and in the moment of contact with surface of sample it would stop, go back a few steps and repeat this process five times. This would create average value

of distance to sample surface which would act as a zero to our measurements. According to datasheet this function should be precise enough to obtain reliable measurement, but as we found out, load range of this function is severely smaller than declared in datasheet, only 7% compared to full range. This value is small compared to random fluctuations in moving resistance that occurs when moving along the linear rails. Therefore we were pushed to abandon this auto-homing function. We believe that we will be able to sort it out in next iteration of this device. Probably our choice of stepper motor with finer steps is disrupting the sensing capabilities of our stepper motor driver.

In light of these findings we moved to a more dummy mode of using the driver. We are still reading missed steps, which is giving red flag in Arduino's serial port output, but no further feedback. We moved parts of auto-homing function to our python master program. We chose to use python instead of C++ which we are using in Arduino control program, because of easy incorporation of measuring card libraries, which interface our voltmeter and voltage source in the measurement card, and also its extensive math library, which we are using to process data, In python program we are using small change in resistance to pinpoint point of contact between our linear stage and sample. This function uses same idea as the one described before.

Our measuring program is rather simple except the auto-homing function. We use serial port communication between python program running on PC and Arduino micro-controller. We are simply telling the Arduino how many steps it should move and looking for any red flags in serial communication(missed steps). From knowing exact number of steps we calculate exact distance moved. We can bend the sample in several iteration, with every iteration we increase strain until total substrate failure.

3. Mechanical simulations

In this chapter we are going to simulate mechanical effects on samples of different substrate materials in our machine. In order to simulate stress, strain and displacement we used simulation tool in Fusion 360 from Autodesk. This allowed us to create detailed simulation of strain and stress distribution and displacement, which helped us with careful planning of mechanical movement in our machine. We are simulating only effects on substrates (350-550 μm), because thickest metal layer applied to these substrates (100 nm) has only negligible effects on overall result and does not add to structural rigidity.

One of the key parameters of our simulations are the constraints, that allow movement of the pushing only in the z axis. Therefore we have only one possible movement of our machine, which corresponds with reality, where the pushing bit is fixed on a moving platform. Another parameter was mesh. We chose to use much finer mesh (0,12 mm grains) on the sample and coarse mesh (0,31 mm grains) with medium mesh on contact surfaces (0,13 mm grains) example of the meshing is shown on Fig 3.1 .

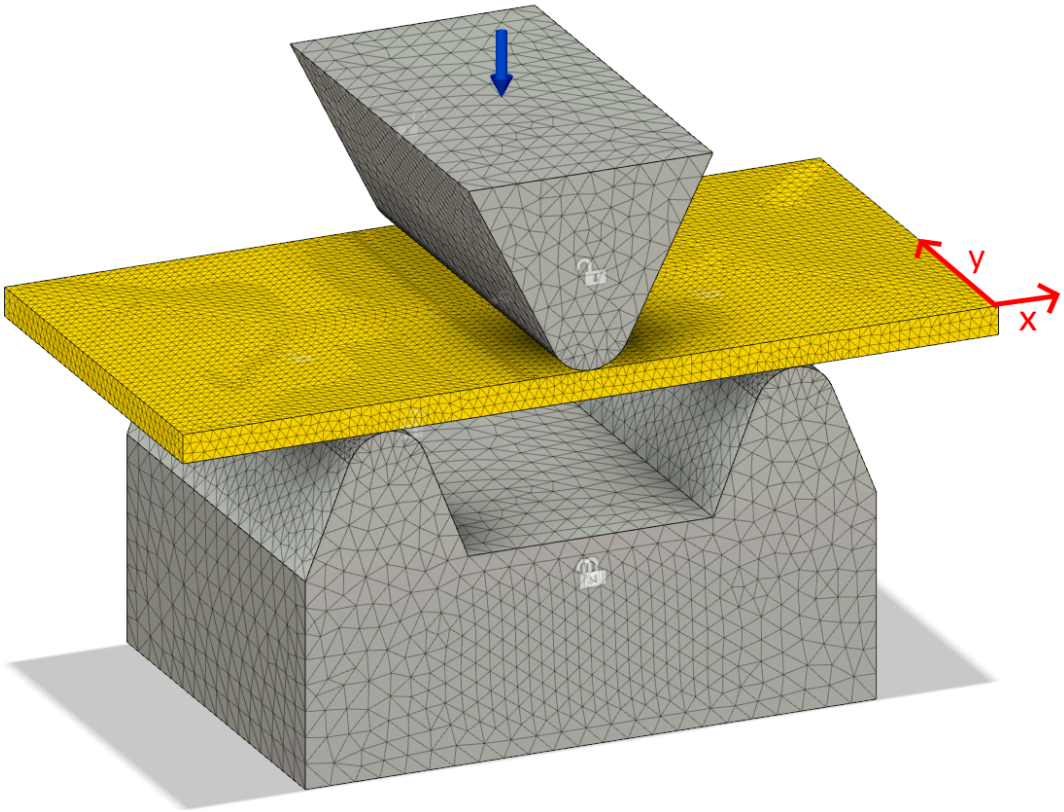

Figure 3.1: Mesh applied to 3D simulation tool in Fusion 360. Sample (yellow) has much finer mesh than machine surfaces.

We have been using moderate force of 40N pushing onto the sample. We chose that, because we have measured our machine developing higher force of 89N. In the simulations we chose to lower that because we wanted to illustrate strain and stress distribution, not to calculate exact maximum before breaking. This was due to breaking of our samples happening much sooner than in theory, which is caused by defects in crystalline structure and uneven surface after wet etching.

3.1 Geometry justification

As mentioned above in section 2.1 rounding the edges of our contact surfaces was mandatory to provide clean bending and reduce risk of breaking the samples. That decision was made by logical argument without any proper calculations at the time of designing the machine. But as we started to do the simulations we wanted to compute effects on sharp and rounded edges and to prove our logical argument of rounding the edges. In order to simulate the effects on the contact edges we were not able to make them as one line, because in real world they have some finite thickness. In order to replicate that we chose rounding them with R=0,005 mm, which can be safely called sharp compared to R=0,5 mm on the rounded ones.

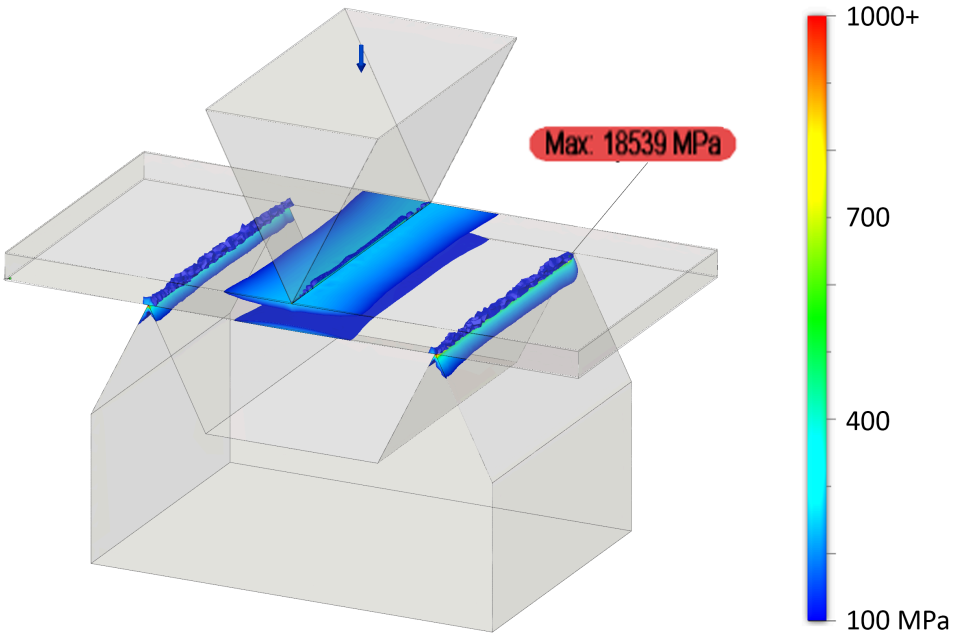

Figure 3.2: Stress distribution with sharp geometry when using pushing force of 40N on GaAs substrate. Point probe shows maximal simulated stress value in the sample.

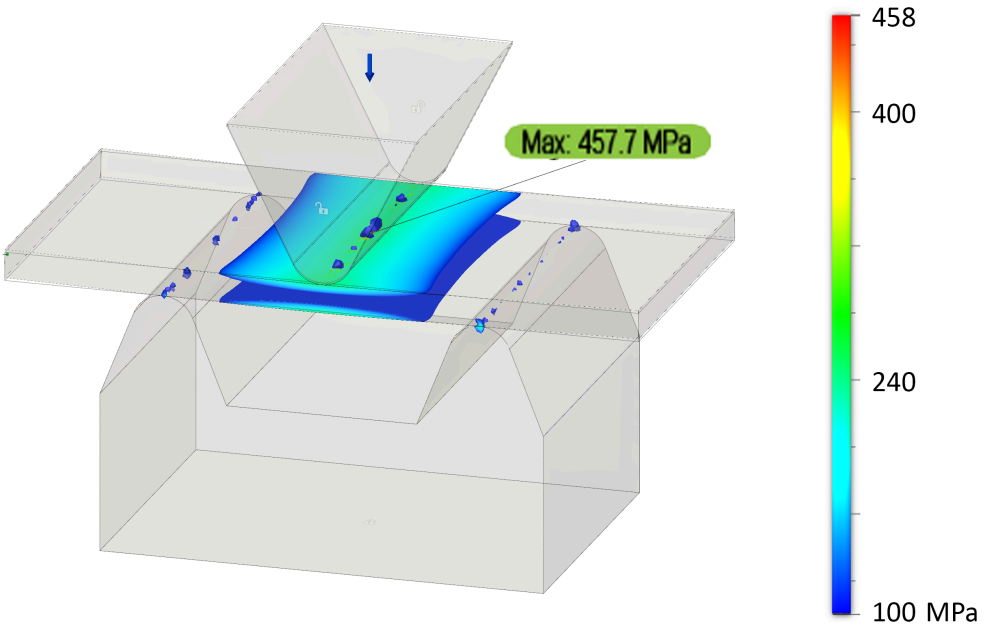

Figure 3.3: Stress distribution with rounded geometry when using pushing force of 40N on GaAs substrate. Point probe shows maximal simulated stress value in the sample.

As we can see stress distribution in the rounded geometry shown in Fig 3.3 is much more even then in the sharp one shown in Fig 3.2. Another thing worth mentioning is that the scale starts at the same stress value in both pictures (100 MPa). Maximum value is concentrated on the surface on the bottom part, but it is wildly different for both geometries. It might be hard to see in the pictures, but in the sharp geometry the maximum stress value is σ=18,5 GPa and compared to that maximum stress value in the rounded geometry is only σ=0,457 GPa which is more than 30 times lower and also is lower than ultimate tensile strength of the GaAs substrate. That is very important, because we want to be able to measure at least 20 points before breaking the sample and with the sharp geometry we move past the breaking point of the substrate rather quickly compared to the round geometry. Due to this we are sure that we made the right argument when we ordered machining of rounded edges on our contact surfaces.

3.2 GaAs substrates

This section is focused on simulations with GaAs substrates with different thicknesses. We are using general mechanical properties of GaAs with orientation [100].

According to [9] [10] [11] these properties at 298K are:
Density ρ = 5,316 g/cm^3
Young's modulus E = 84,9 GPa

Poisson ratio ν = 0,312
Elastic anisotropy factor a = 0,547
Shear modulus C'= 32,85 GPa
Yield strength = 1,5 GPa
Tensile strength = 2,1 GPa
Thermal conductivity χ = 0,58 W/(cm.K)
Thermal expansion coefficient $\alpha = 5{,}6 \cdot 10^{-6}$ K^{-1}
Heat capacity C_P = 0,327 J/(g.K)

We have done simulations for different thicknesses of our GaAs substrates, because according to manufacturer of our substrates it has thickness of 350 μm +- 50 μm and 500 μm +- 50 μm. Therefore, we chose to simulate these thicknesses : 350 μm , 450 μm and 550 μm. As you will see there is not much of a difference in strain and stress distribution.

Looking at results of these simulations have provided us with a few key parameters. Maximum induced strain is in the center of the sample, where we are measuring electrical resistance. Maximum induced stress caused by applying constant force of 40N is used to determine breaking point of the sample. And lastly it had provided us with displacement of the center part of the sample.This helps us determine number of steps needed to safely bend the sample and also to judge whether is it worth to test this specific substrate. Because if we knew that we can only obtain 5 measuring points before breaking the sample, it would be a signal to change something in our measurement in order to make it more precise. We are aiming at least for 25 data points.

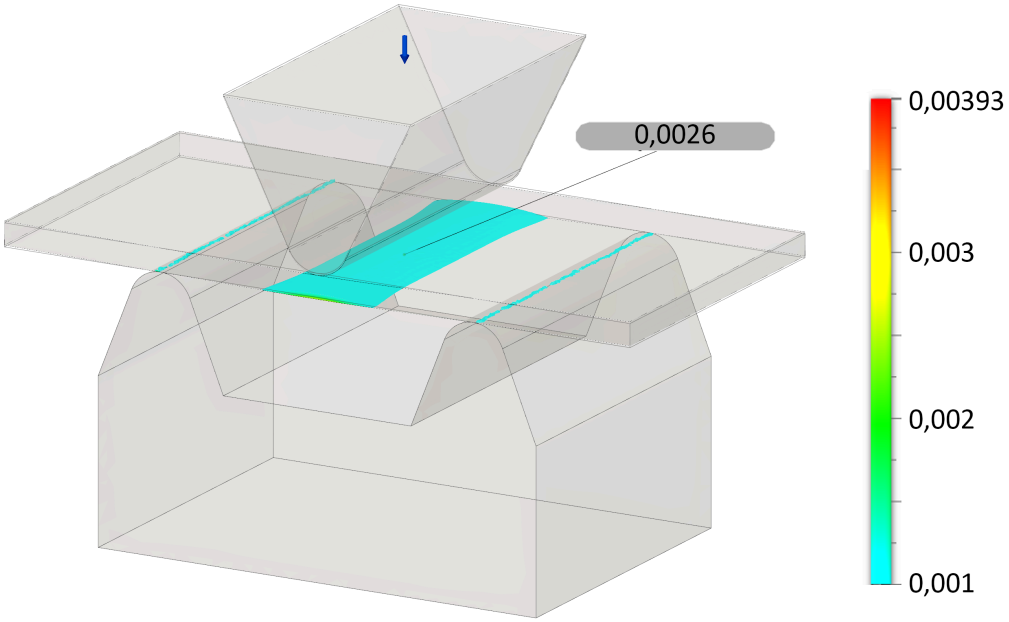

Figure 3.4: Strain distribution along x axis in 350 μm GaAs substrate with force of 40N applied. Point probe shows strain in the parts where device is located.

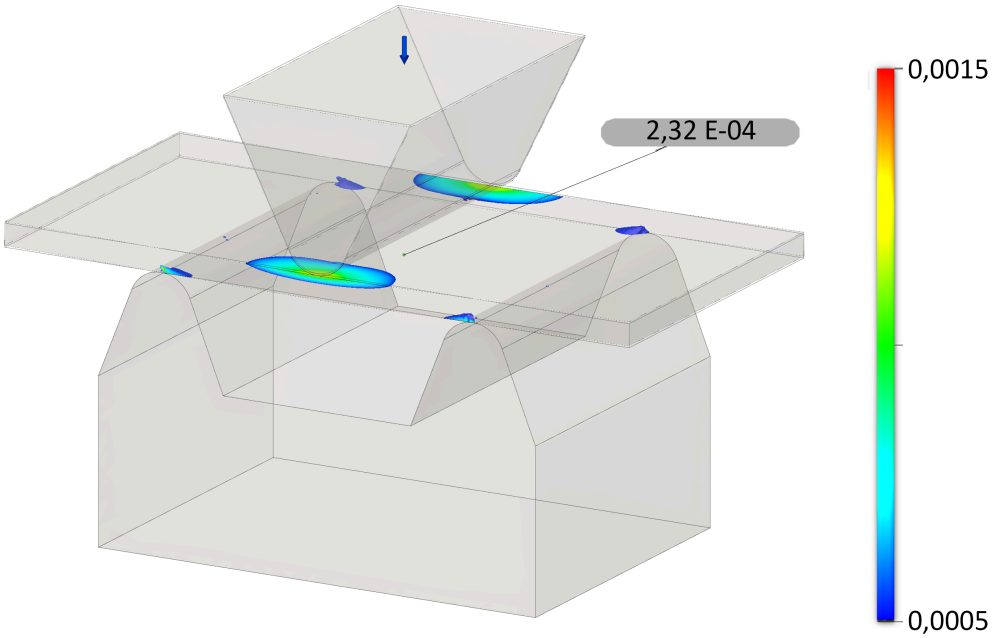

Figure 3.5: Strain distribution along y axis in 350 μm GaAs substrate with force of 40N applied. Point probe shows strain in the parts where device is located.

As we can see on Fig 3.4 and in table 3.1, strain distribution along the x axis (longer side of the sample) is in the center more or less homogeneous. This is supporting our intention to use centered diagonal cross for measuring changes in electrical resistance. We can also see, that the maximum strain is induced in the center of the sample, with almost no strain in direction perpendicular to the x axis (compare between figures 3.4 and 3.5). Looking at the table 3.1 we can state that GaAs is the most suitable substrate from our range of substrates for bending purposes. Because we can create the highest strain with constant force applied and since GaAs is less brittle compared to GaP it makes it the best candidate for application of thin metal films.

3.3 GaP substrates

This section is focused on simulations with GaP substrates with different thicknesses. We are using general mechanical properties of GaP with orientation [110].

According to [12] these properties at 300K are:
Density $\rho = 4{,}14$ g/cm^3
Young's modulus E = 103 GPa
Poisson ratio $\nu = 0{,}31$
Shear modulus C'= 39,2 GPa
Yield strength = 0,6 GPa (used in simulation, approximated from higher temperature measurement)
Tensile strength = 1 GPa (used in simulation, approximated from higher temperature measurement)
Thermal conductivity $\chi = 1{,}1$ W/(cm.K)
Thermal expansion coefficient $\alpha = 4{,}65 \ . \ 10^{-6}$ K $^{-1}$
Heat capacity $C_P = 0{,}43$ J/(g.K)

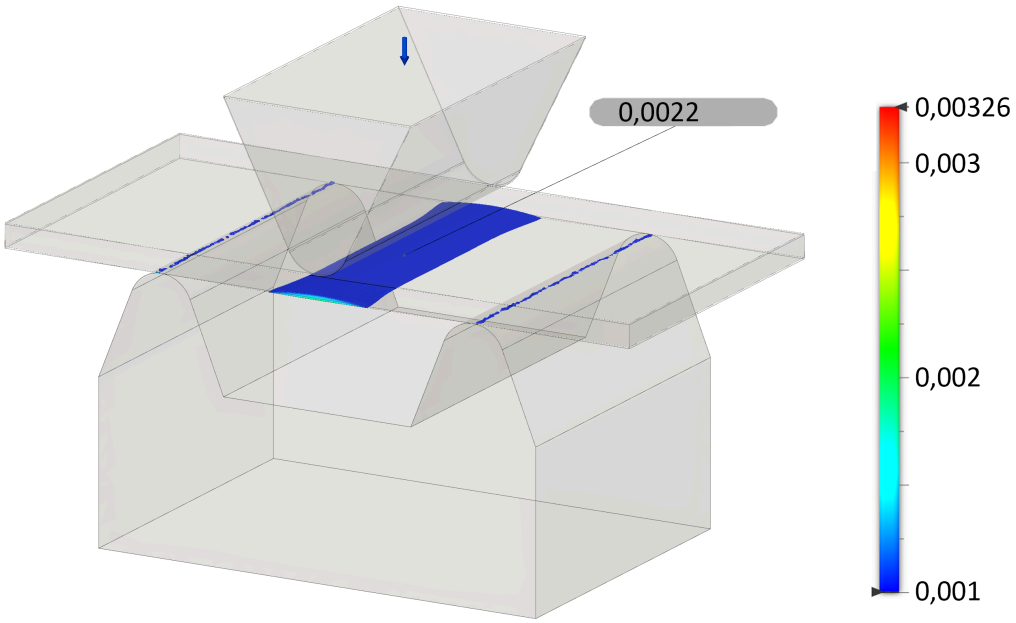

Figure 3.6: Strain distribution along x axis in 350 μm GaP substrate with force of 40N applied. Point probe shows strain in the parts where device is located.

3.4 Comparisons of different substrates

We compared simulations for different substrates. We will be using devices mainly on GaAs substrate, but we will measure some on much more expensive GaP substrate. Simulations showed better stiffness and therefore lower strain on GaP

substrate. But the difference is not that high to prefer one substrate to another. Displacement also shows we would be able to collect enough data points to do a reasonable experiment, since we are taking data every 2,5 μm. All simulation results are shown in Tab. 3.1.

First two columns show substrate type and simulated thickness. In the third column is simulated strain in the center of the sample, which is where our device is located. Maximum strain represents maximal computed strain overall on the whole sample. Maximum stress has the information whether the sample will break or not, if we compare it to the tensile strength of given material and displacement column represents how much the center of the sample moves in the pushing direction.

Substrate	Thickness [μm]	Strain in center [‰]	Maximum strain [‰]	Maximum stress [MPa]	Displacement [μm]
GaAs	350	2,59	7,38	693	29,8
GaAs	450	3,39	4,49	669,1	30,39
GaAs	550	1,91	3,96	476,4	14,44
GaP	350	2,16	6,12	691,2	24,77
GaP	450	2,85	4,18	654,9	25,57
GaP	550	1,60	2,47	574,5	12

Table 3.1: Simulations results for used GaAs and GaP substrates with 40N pushing force applied.

4. Sample fabrication

In this chapter we will tackle the process of sample fabrication from a substrate to a finished sample. Creation of the samples involved few highly specialized processes. These include an optical lithography, a metal deposition and a metal lift-off. In order to prepare good enough samples we needed to optimize all of these processes.

4.1 Substrate preparation

We decided to use samples with dimensions 10x5 mm^2. We started with quarters of two inch substrates (of GaAs and GaP). Therefore we needed to be creative in placing our 10x5mm regions on the shards. We used scratching machine with diamond stylus to create grooves in substrates as in Fig 4.1. Then we bent substrates along the sharp edge and they broke along the scratched line. Scratching machine is equipped with microscope and moving platform which has indicators in 10μm intervals. This enables us to get precise dimensions of our substrates.

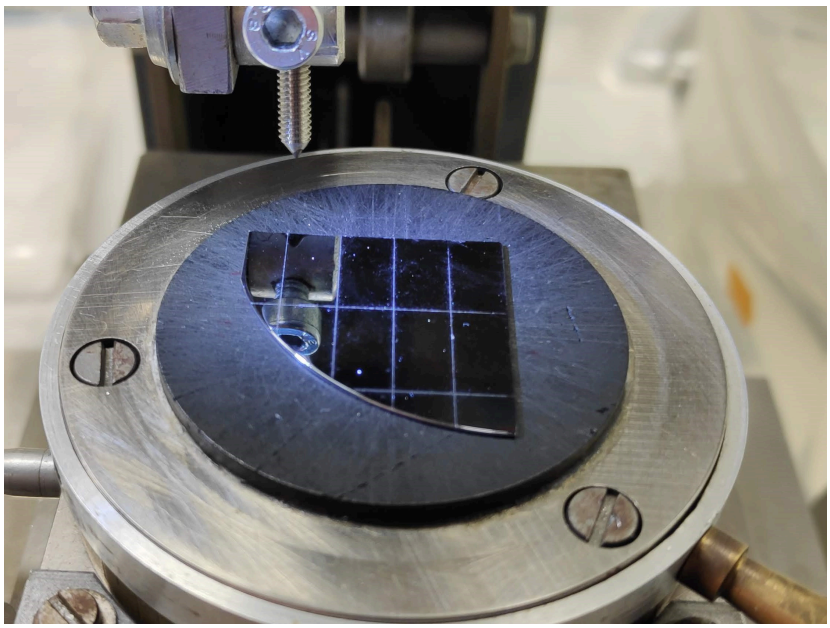

Figure 4.1: GaAs substrate with scratched lines before it was broken into individual samples.

4.2 Optical lithography

In order to use the optical lithography firstly we needed to create mask for it. That was created using the Electron Beam Lithography machine (EBL). We used plane of glass coated with special blend of copper and gold with anti-reflection layers. This helps to minimize interference and stray reflections in UV region and help with creating precise distinction between irradiated and non-irradiated surface of sample underneath the mask. Our mask took nearly 14 hours of exposition time in EBL. After that it was developed and etched in oxygen plasma and all non-exposed parts of metal coating were washed away.

When creating our samples we used a optical resist ma-N 1410 from Micro resist technology [13]. This resist is negative resist (hardens in the parts exposed to UV) with optimal properties for lift-off metal coating application. This resist is sensitive in the UV region of 300-410 nm and thermally stable up to 160°C.

4.2.1 Our working process of optical lithography

When working with the optical lithography our laboratory is equipped with a clean room. This helps in keeping substrates clean from any dust and other particles. Firstly we clean substrates with acetone, then deionized water and we dry them using compressed nitrogen gas. After this process we prepare small amount of negative tone photoresist into the pipette. We have been using ma-N 1410 for that. Using spincoating technique set for 3000rpm and 40s we create photoresist coating with thickness of 1μm, which is more then adequate for metal lift-off of less than 100nm thick films. After spincoating we bake the resist layer on a hotplate set up to 100°C for the period of 90s.

After successful preparation of the photoresist film we insert the sample into the optical lithography machine under the prepared mask. We use included microscope to align the mask and coated substrate. After that we start the exposure which is automatically set to a certain dose. We move exposed samples into the development agent, in our case ma-D 533S for 40s followed by rinse in deionized water and drying with nitrogen gas.

4.3 Metal deposition and lift-off

After successful resist application and optical lithography we move towards metal deposition. We are equipped in our laboratory with the metal deposition machine. We can create thin metal films by evaporating pure metal in a high vacuum. We place samples in a rotating sample holder. Then we place the holder inside the chamber of the deposition machine and start the central vacuum pump along with a turbomolecular pump. With this combination we are able to achieve pressures in 10^{-7} torr. This can be achieved after only 8-10 hours. When we are happy with achieved pressure inside the chamber we start to heat up desired metal for our application. We are measuring the material flow on a weight sensitive crystal and it is measured in Å/s. When rate stabilizes we open the shutter shielding our samples, reset the layer thickness counter and wait till layer thickness counter reaches desired value. Then we close the shutter and turn off power for heating the pure metal. We then have to wait for at least 15min for chamber to cool

down and only after that we can continue by turning off the vacuum pumps. After chamber reaches atmospheric pressure we are able to open it and remove the sample holder.

Deposited metal film is still on the whole sample and we need to remove photoresist along with parts of the metal film. We do that in acetone, which is a good solvent for our types of photoresists. In order to do this process faster we place glass container with acetone and our sample inside ultrasonic bath for at least 20min. Ultrasound helps with freeing metal layer away from our sample. Then we rinse the sample in deionized water and dry it with nitrogen gas.

For this measurements we chose to deposit Chromium, Nickel and Nickel-Chromium (Ni 80% Cr 20%). These metals are interesting for us because we know constants of Nickel and NiChrome, they can be found in Table 1.1 and Chromium is interesting for its antiferromagnetic properties. It is one of the materials in interest of our research group at Czech Academy of Sciences.

We were able to deposit 30nm of Chromium. Thicker layers are much more difficult to deposit, because Chromium is deposited at higher temperature and after a while the whole chamber starts to heat up and gases trapped inside chamber walls break free and tamper with the vacuum inside the chamber. Thicker layers are only possible after longer degassing period - pumping for more than three days.

As per Nickel, we chose to deposit 30nm of it, to be consistent with previously made samples of Chromium. We chose it for its interesting property of having negative dependence of electrical resistance on strain. We were curious to see that in real life, so we chose Nickel.

And lastly as a comparison with industrially used material we tried to create NiChrome in ratio of 80% Ni and 20% Cr. This material is commonly used in strain gauges and resistance wires. Therefore it was rather easy to find resistivity values for this material.

4.4 Sample inspection under optical microscope

After creating first batch of samples with applied Chromium we decided to inspect them under optical microscope. We have found out few of our mistakes, greatest one being pausing the lift-off process by puling sample out of acetone. That can be seen on Fig 4.2. Comparing the edges of chromium layer on GaP substrate on Fig 4.2 and 4.3 we can see great impact that pulling out of acetone had on quality of the sample.

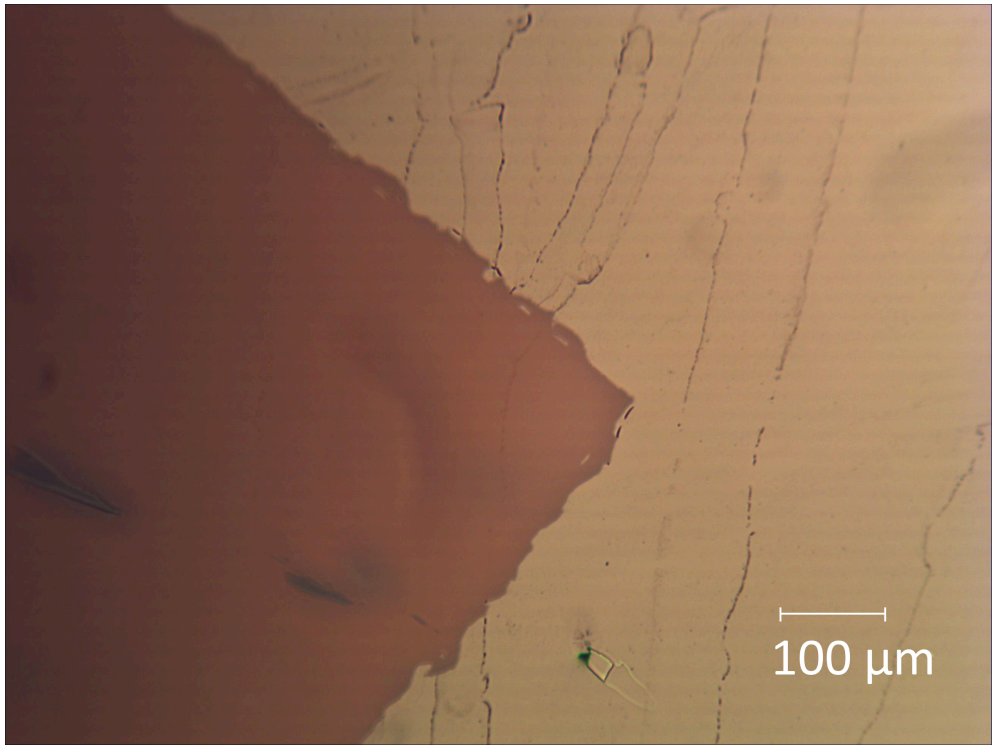

Figure 4.2: Botched metal lift-off on sample of 30nm thick chromium(yellow) on GaP substrate. 10x magnification

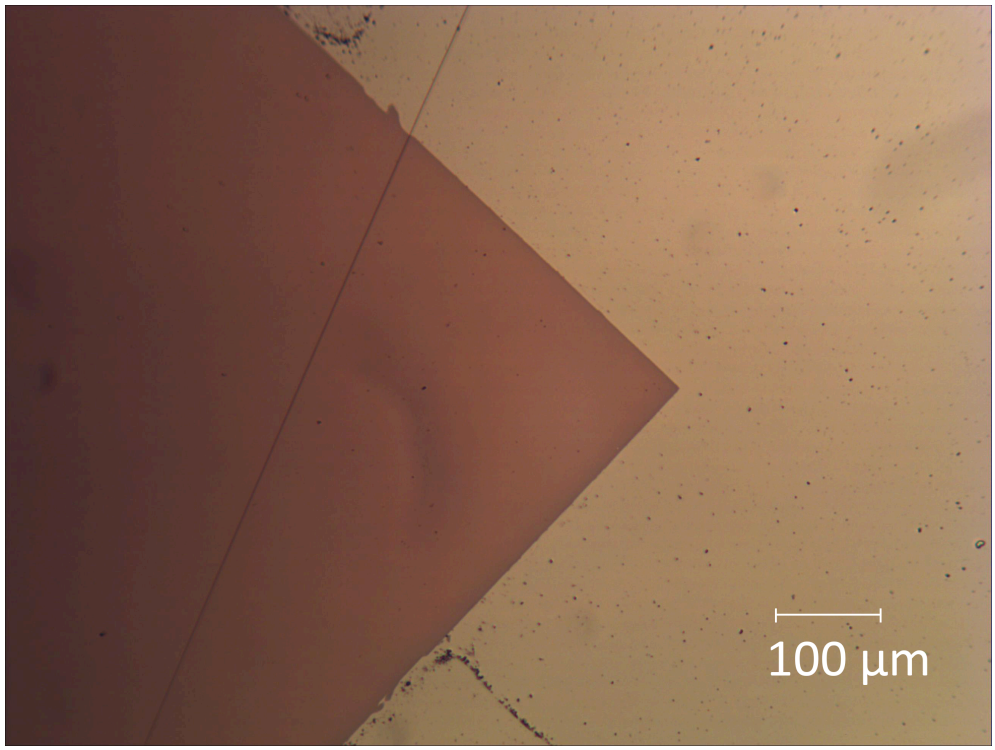

Figure 4.3: Proper metal lift-off on sample of 30nm thick chromium(yellow) on GaP substrate. 10x magnification

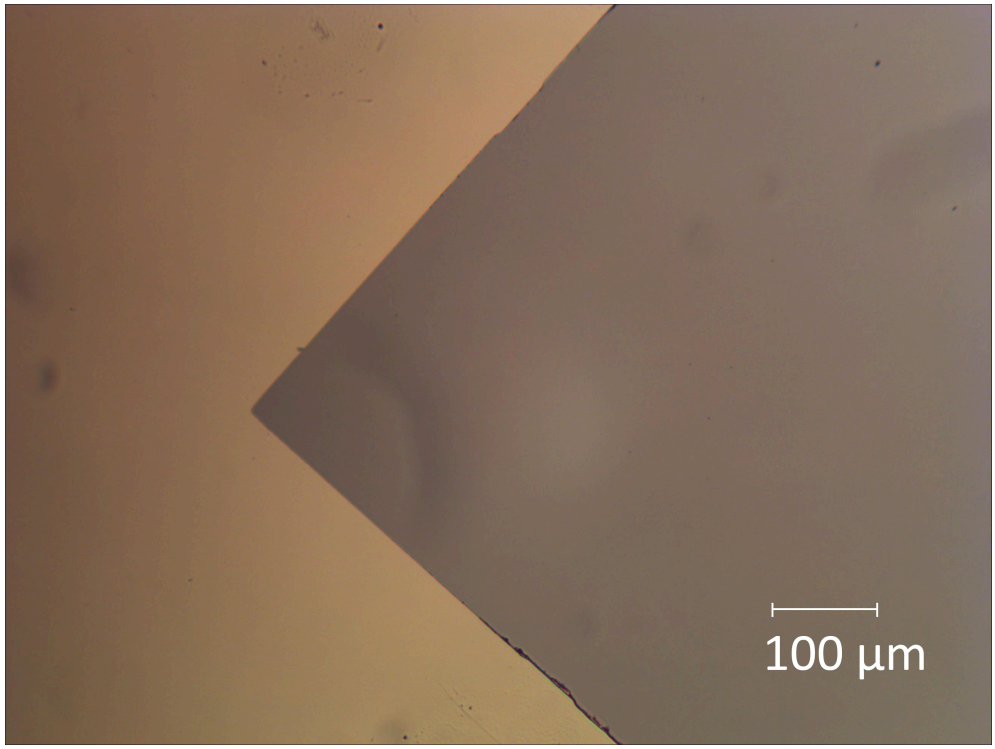

Figure 4.4: Proper edge of 30nm thick chromium(yellow) on GaAs substrate. 10x magnification

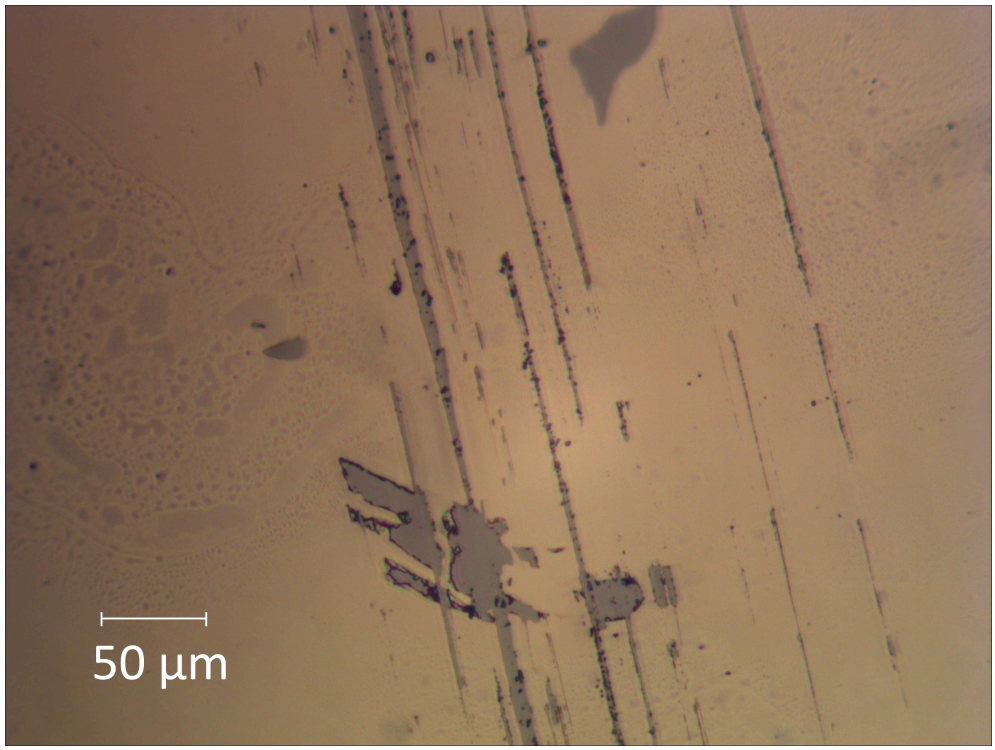

Figure 4.5: Example of scratches in GaAs substrate manifesting after application of 30nm chromium(yellow) film. 20x magnification

We can see nice uniform layer of chromium(yellow) on Fig 4.4 with precise edge. This is our target sample quality. But as we did not use oxygen plasma in order to clean substrates from small particles and scratches. We encountered manifestations of a scratched substrate in visible lines destroying continuity of chromium film Fig 4.5. Therefore after first batch of samples we started to use oxygen plasma in process of substrate preparation.

5. Measurement

In this chapter we will focus our attention on the measurement. We will show graphs of raw and analyzed data and come to the conclusions in determining material constants for each of the tested materials.

5.1 Measurement process

First of all we aligned the sample onto contacts. As a verification we have measured two point and four point resistance for both directions - strained horizontal and non-strained vertical direction. This was determining our starting resistance and also showing us whether we positioned sample correctly on top of the contact needles.

After we verified proper sample placement we started automated python script which initialized readout card, arduino, connection matrix and started pushing on the sample. We used two different types of pushing patterns.

In order to give sample time to cope with induced material stress we chose "up and down" method. In this we moved 5 steps down (12.5μm) and 4 steps up (10μm). This we repeated and number of repetitions determined ultimate distance we were able to push on the sample. Compared to our other method, which consisted only from pushing down until sample broke we were able to push around 20-50μm more. That points out that doing slow and flexing measurement allowed the sample to better cope with the induced stress and also data pointed out that it allowed the sample to slide a bit on the edges.

Firstly we focused on the data in direction of putting in the pressure. Therefore we chose only those measurement points when motor was pushing onto the sample. And since we have measured every step value five times (because of up down methodology) we did mean of those values. In the end we ended up with one value per step.

Now we can determine three regions as can be seen on Fig. 5.2. First almost flat region corresponds to sample slowly closing on the bending edges. Second with slow rise corresponds to slight bending of the sample and flexing of the plastic parts and third, much steeper region corresponds to bending of the sample after plastic parts had already flexed. Point where first region meets with second is taken as a reference point to get step value for 0 strain and we calculate strain (s) from distance between current step value and our zero point using this formula:

$$s = (P - P_0) \cdot k \tag{5.1}$$

Where P represents position in step number, P_0 represents interpolated step value for 0 strain, constants k were determined from simulations in chapter 3 for given thickness of substrates. $k_{GaAs} = 2,75{\cdot}10^{-4}$ and $k_{GaP} = 2,81{\cdot}10^{-4}$ These were used because calculation of strain in certain area is not well defined. Substrate is not bending along the perfect circle and straining uniformly, but rather concentrating most of the strain in approximately 1mm wide region in the centre of the sample. This was determined from simulations and later used in our experiments.

Smoothing the data was giving a noticeable improvement in their clarity and interpretability. As we can seen on Fig. 5.1 which shows raw data in time with

the step counts, showing previously discussed measurement process. Comparing it to Fig. 5.2 having only data in pushing direction, which have been averaged between measurement points belonging to one step value. This data shows three basic trends. Two interesting ones are straining with elastic deformation and rapid increase of resistance due to lower flexing of the plastic parts and actually bending the substrate.

Prominent effect apparent on Fig. 5.3 are the contact point problems. Those are apparent mostly on a single direction sweeps, but they happen randomly. We believe that these spikes visible on Fig. 5.3 are caused by temporary loosing electrical contact between the needle and the sample, but also this spike can be attributed to the slowly acting spring inside contact needles that was not able to keep the constant pressure applied to the sample.

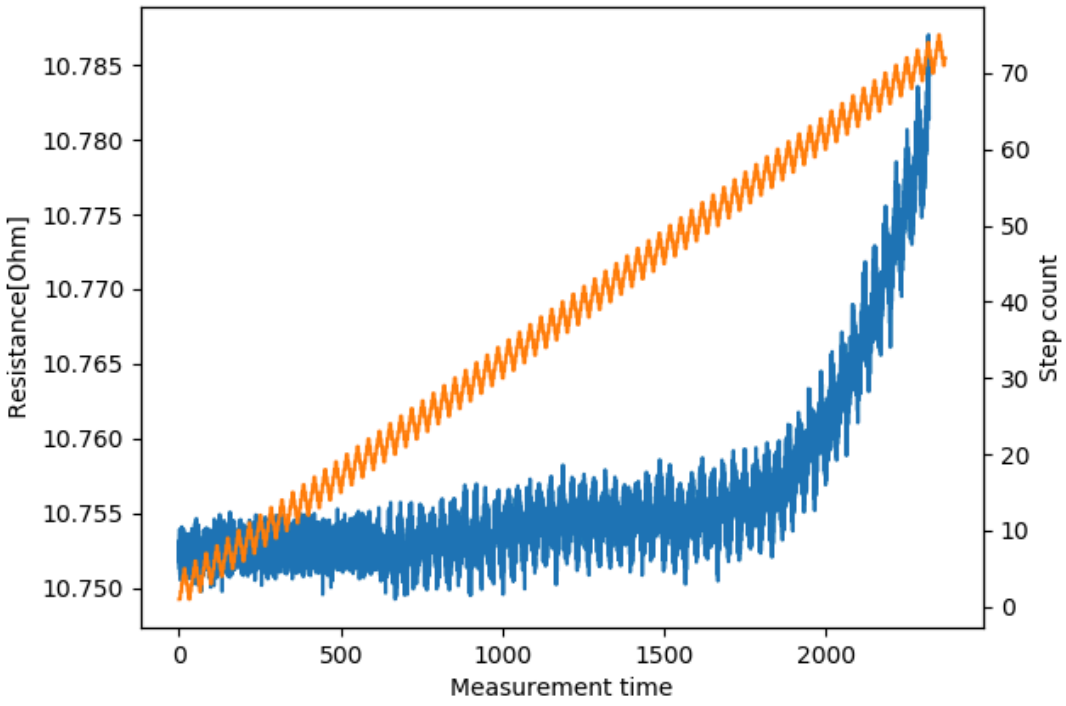

Figure 5.1: Raw data for Cr sample 1 on GaAs. Here we can see all phases of deformation in substrate.

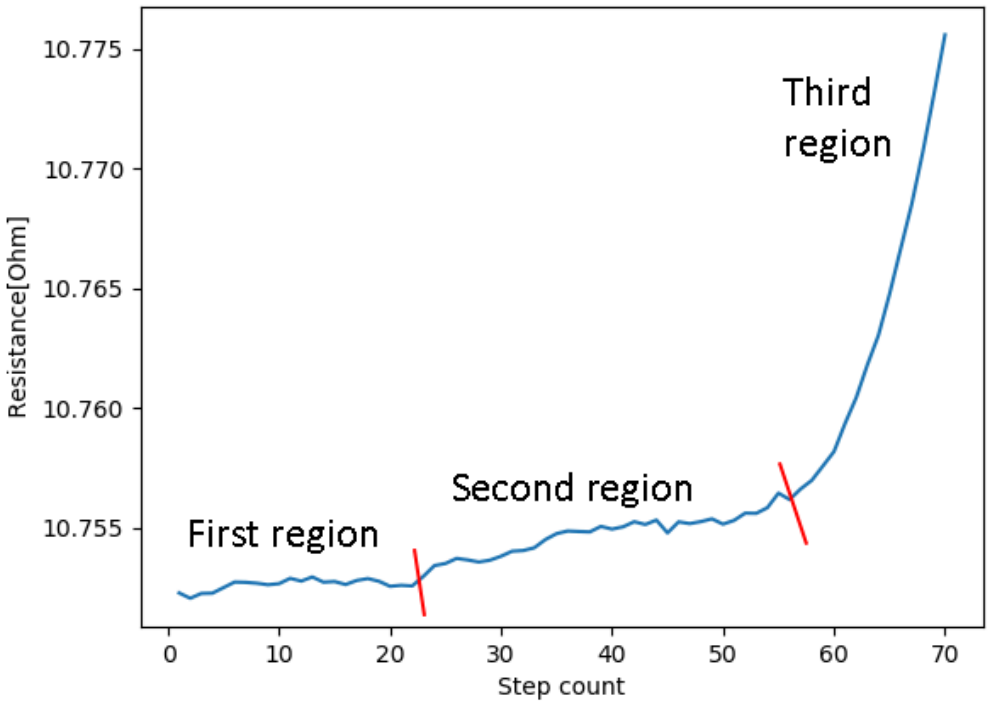

Figure 5.2: Processed data for Cr sample 1 on GaAs.

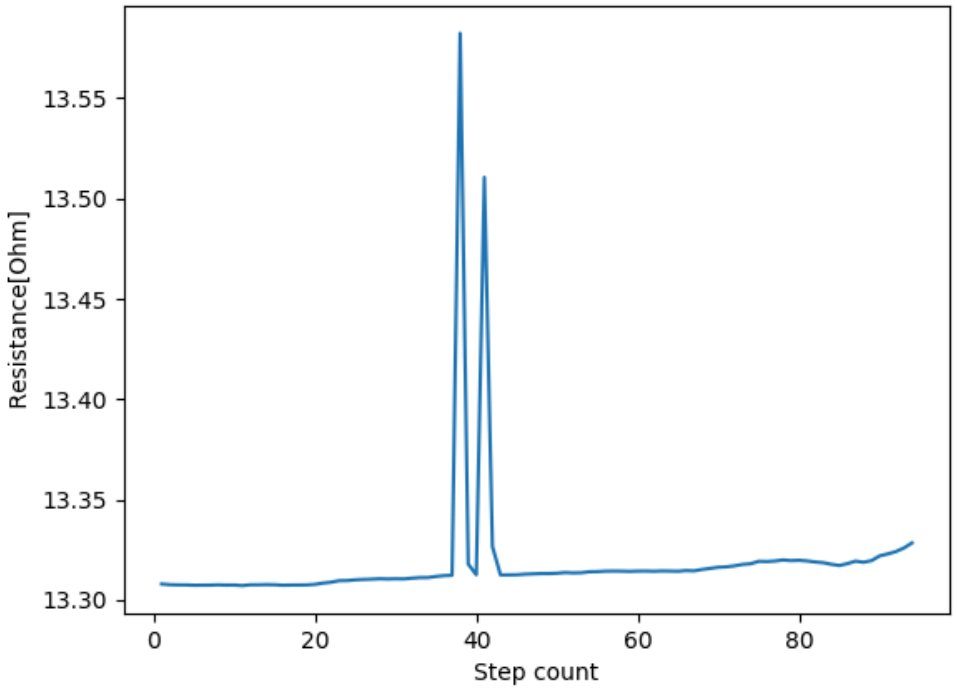

Figure 5.3: Processed data for NiCr sample 3 on GaP. This shows problems with contact points.

5.2 Data interpretation and gauge factor

As we started to interpret measured data we found out that the effects of lowering stress in the samples are hugely present. As we can see in Table 5.1 and 5.2, measured material constants for known materials are lower than the ones available in literature for both Gauge factor 1 and 2. Difference between them is in fitting region. Gauge factor 1 is fitted for whole measured resistance curve including both trends - slow rise and steep rise before breaking. In contrast gauge factor 2 is fitted only for steep end of the curve as in Fig. 5.2. This was done because we suspect that in this region plastic parts have been flexed and are not flexing as much anymore. Not every sample had this part of the measured curve, therefore we suspect it broke sooner then the plastic flexed.

Therefore the difference is probably not result of detailed imperfections (contaminations etc.) of our films. It is more likely that strain relieve effects were in progress during measurements. We summarize several effects which most likely contribute to this non-linear dependency measured:

1. Flexing in the plastic parts of our machine.
2. Maxiumum strain is not properly distributed throughout the whole active area on the sample.
3. Placement of the sample - measured device (cross) might have been a bit off center resulting in lower strain applied to it.
4. Sliding along the edges resulting in movement of the whole sample.
5. Pre-straining of samples happening because of needle contacts pushing against the sample.

Sample	Max. nominal strain [‰]	Relative resistance change [‰]	Gauge Factor 1	Gauge Factor 2
NiCr1	12,20	0,83	0,068	0,529
NiCr2	16,08	0,83	0,052	0,299
NiCr3 (GaP)	20,79	1,58	0,076	0,331
NiCr4	5,60	0,50	0,088	0,287
NiCr5	6,04	1,54	0,256	0,415
Cr1	6,80	2,18	0,320	1,171
Cr2	11,87	2,69	0,227	0,890
Cr3 (GaP)	12,11	0,92	0,076	0,165
Ni2	15,49	-4,75	-0,307	did not have
Ni3	7,02	-0,42	-0,060	-0,425
Ni4 (GaP)	12,65	-1,05	-0,083	did not have

Table 5.1: Results for different metals measured with updown technique.

Another thing to note is quite broad spectrum of values of maximal achieved nominal strain. Its variation can have instrumental origin (ireproducibility of flexing of the plastic parts) however we believe it is quite likely consequence of particular properties of scratching and cleaving edges of the samples.

The second method of pushing was simple up sweep. In that we did the pushing movement in one direction only. The results of these measurements are summarized in Tab. 5.2. With this method we achieved lower step counts for sample breaking resulting in higher Gauge Factor better fitting the expectations.

This points out that in the updown method samples and the apparatus have time and a lot of small movements to perform deformations of various types. However the measurement with the simple up sweep method was heavily disturbed by bad connections of contact pins which was suppressed with the updown method.

We can conclude that the updown method seems more promising for the future measurements of spintronic samples since it provides more reliable electrical connection while the actual value strain can be determined from the resistance of the device.

Sample	Max. nominal strain [‰]	Relative resistance change [‰]	Gauge Factor 1	Gauge Factor 2
Cr4	5,6	1,93	0,344	1,20
Cr5	4,1	0,71	0,173	did not have

Table 5.2: Results for different metals measured with single sweep technique.

6. Discussion and possible improvements

Some of the problems we discovered were already mentioned in previous chapter and we will try to address them and conceive solutions to these problems.

6.1 Contacts

The most noticeable problem was sudden change in resistance due to moving of the contact needle. We have proved that gluing contacts can mitigate the problem, but it is time consuming and adds problems created by glue residue. So we focus now how to improve current setup.

First of all, we advise to use gold layer on every contact pad. High conductivity and elasticity of gold will help mitigate defects in layer underneath like cracks and scratches. This can be very beneficial as even 50nm layer of gold will bridge any defects or scratches on the surface of the sample. This will also provide cushion for needles to bite into. If a needle pushes deep enough into the gold layer it will create much more secure contact than with relatively hard metal layer we had on previous samples.

If we decide to improve electrical contacts even further, we would like to try few different types of flexible/spring loaded contacts. Since we think our contact needles are slightly scratching the surface, we would like to try rounded spring loaded contacts. Another thing to improve is the contact placement, we need to try getting the contacts into the same height in order for them to apply same pressure. Interesting thing to try would be contacts from flexible metal strips. They have much larger contact area, which could help maintain good contact through the whole measurement.

6.2 Material choices

As we have shown in the previous chapter, gauge factor is much lower than expected. This is mainly because only 10-20% of induced motion is successfully transferred to the sample where it creates strain. We see a lot of improvement achievable in that regard, because we can see change in trend after plastic stops flexing as much. We would like to stiffen the machine using blend of aluminum and plastic parts. We are trying to get access to available CNC machine and machine bottom part of our bending machine from aluminum. This is in our eyes the weakest part of the whole design since only plastic is supporting stainless steel edges on which the samples are bent. We would also suggest using linear rails to guide the moving part instead of metal rods with linear bearings. This will also help stiffen the whole machine.

6.3 Readout improvements

In further measurements we plan to include measurement also in direction perpendicular to the bending and diagonal direction. We also want to try different motor speeds and movement patterns in order to find perfect balance between number of gathered points and letting the sample to cope with applied force over time. We also believe that better golden contacts will help with our readout.

Conclusion

Specialized machine capable of inducing mechanical strain into thin layers on top of different substrates was designed and constructed. This machine was thoroughly tested in order to find weak spots of our design and to evaluate its capabilities.

During construction only commercially available parts were used. For mechanical construction mostly plastic was used, due to availability of 3D printing. This allowed us to create our design relatively fast. The presence of plastic parts came with crucial disadvantage - plastic parts can flex during the bending process.

Electrical measurements of 30nm thick films of three materials - NiCr, Cr and Ni were conducted. They have showed:

1. Machine is capable to go beyond ultimate tensile strength of GaAs and GaP substrate materials used in our department.

2. We are able to change strain with steps of reasonable size before breaking the sample, therefore giving us enough data for later processing.

3. Measured dependency of resistance on strain is not linear, which we attribute to usage of plastic parts in machine construction and their deformation.

During making of this thesis we were able to learn many experimental and manufacturing skills including:

1. Proper manipulation with wafers used in MBE machines and how to cut them.

2. Electron beam lithography used to create optical lithography masks.

3. Using of optical lithography to create devices from thin layers on substrates.

4. Evaporative metal deposition.

5. Optical and electron beam microscopy.

6. Programming in C++ and Python in order to create mostly automated experiment.

7. Using of CAD software Fusion 360 used to design all parts of our machine.

8. Using computer simulations to improve mechanical design of our machine.

9. Using of a 3D printer. (Tinkering with different plastics, infill patterns and ratios to obtain strongest possible parts etc.)

If the future experiments with the spintronic devices open potentially new direction of looking at our current working material CuMnAs. We will rebuild the weakest parts of our machine. Starting with using more metal in the construction and change in contact needles.

Bibliography

[1] John H. Lienhard Thomas G. Beckwith, Roy D. Marangoni. *Mechanical Measurements*. Addison-Wesley Publishing Co, 2006.

[2] Ali M. Sadegh Warren C. Young, Richard G. Budynas. *Roark's Formulas for Stress and Strain, Eighth Edition*. The McGraw-Hill Companies, Inc., 2012.

[3] Michael B. Heaney. *"Electrical Conductivity and Resistivity." Electrical Measurement, Signal Processing, and Displays*. CRC Press, 2003.

[4] K. Výborný J. Zemen J. Mašek Aurélien Manchon J. Wunderlich Jairo Sinova J. Železný, H. Gao and T. Jungwirth. Relativistic néel-order fields induced by electrical current in antiferromagnets. *PHYSICAL REVIEW LETTERS*, 113, 10 2014.

[5] P. Wadley, B. Howells, J. Železný, C. Andrews, V. Hills, R. P. Campion, V. Novák, K. Olejník, F. Maccherozzi, S. S. Dhesi, S. Y. Martin, T. Wagner, J. Wunderlich, F. Freimuth, Y. Mokrousov, J. Kuneš, J. S. Chauhan, M. J. Grzybowski, A. W. Rushforth, K. W. Edmonds, B. L. Gallagher, and T. Jungwirth. Electrical switching of an antiferromagnet. *Science*, 351(6273):587–590, 2016.

[6] Wantai motor. Wantai mini stepper product specifications. `http://www.electronicaestudio.com/docs/SHT-143.pdf`. [Accessed: 2019-02-10].

[7] Trinamic. Tmc2130-la datasheet. `https://www.trinamic.com/fileadmin/assets/Products/ICs_Documents/TMC2130_datasheet.pdf`, May 2018. [Accessed: 2019-01-10].

[8] Prusa Polymers. Technical datasheet prusament pla. `https://shop.prusa3d.com/cs/index.php?controller=attachment&id_attachment=20`, Sep 2018. [Accessed: 2019-02-19].

[9] Dargys A. and J. Kundrotas. *Handbook on Physical Properties of Ge, Si, GaAs and InP*. Science and Encyclopedia Publishers, Vilnius, 1994.

[10] C.P.Chen. *Fracture mechanics evaluation of GaAs*. NASA, Jet Propulsion Lab., California Inst. of Tech., 1984.

[11] T. Tokuoka & I. Yonenaga T. Suzki, T. Yasutomi. Plastic deformation of gaas at low temperatures. *Philosophical Magazine A*, 79, 1999.

[12] Ioffe Institute. Gap properties. `http://www.ioffe.ru/SVA/NSM/Semicond/GaP/index.html`. [Accessed: 2019-03-19].

[13] Microresist technology. ma-n 400 & ma-n 1400 series. `https://www.microresist.de/en/products/negative-photoresists/uv-lithography-broadband-and-i-line-exposure/ma-n-400-ma-n-1400`. [Accessed: 2019-04-04].

List of Figures

List of Tables